



**HAL**  
open science

## Search for $^{22}\text{Na}$ in novae supported by a novel method for measuring femtosecond nuclear lifetimes

Chloé Fougères, François de Oliveira Santos, Jordi José, Caterina Michelagnoli, Emmanuel Clément, Yung Hee Kim, Antoine Lemasson, Valdir Guimarães, Diego Barrientos, Daniel Bemmerer, et al.

### ► To cite this version:

Chloé Fougères, François de Oliveira Santos, Jordi José, Caterina Michelagnoli, Emmanuel Clément, et al.. Search for  $^{22}\text{Na}$  in novae supported by a novel method for measuring femtosecond nuclear lifetimes. Nature Communications, 2023, 14 (1), pp.4536. 10.1038/s41467-023-40121-3 . hal-03912454v1

**HAL Id: hal-03912454**

**<https://hal.science/hal-03912454v1>**

Submitted on 24 Dec 2022 (v1), last revised 20 Aug 2024 (v2)

**HAL** is a multi-disciplinary open access archive for the deposit and dissemination of scientific research documents, whether they are published or not. The documents may come from teaching and research institutions in France or abroad, or from public or private research centers.

L'archive ouverte pluridisciplinaire **HAL**, est destinée au dépôt et à la diffusion de documents scientifiques de niveau recherche, publiés ou non, émanant des établissements d'enseignement et de recherche français ou étrangers, des laboratoires publics ou privés.



Distributed under a Creative Commons Attribution 4.0 International License

# Search for $^{22}\text{Na}$ in novae supported by a novel method for measuring femtosecond nuclear lifetimes

C. Fougères<sup>1,2\*</sup>, F. de Oliveira Santos<sup>1\*</sup>, J. José<sup>3,4</sup>, C. Michelagnoli<sup>1,5</sup>, E. Clément<sup>1</sup>, Y.H. Kim<sup>1,6</sup>, A. Lemasson<sup>1</sup>, V. Guimarães<sup>7</sup>, D. Barrientos<sup>8</sup>, D. Bemmerer<sup>9</sup>, G. Benzoni<sup>10</sup>, A.J. Boston<sup>11</sup>, R. Böttger<sup>9</sup>, F. Boulay<sup>1</sup>, A. Bracco<sup>10</sup>, I. Celikovic<sup>12</sup>, B. Cederwall<sup>13</sup>, M. Ciemala<sup>14</sup>, C. Delafosse<sup>15</sup>, C. Domingo-Pardo<sup>16</sup>, J. Dudouet<sup>17</sup>, J. Eberth<sup>18</sup>, Z. Fülöp<sup>19</sup>, V. González<sup>20</sup>, J. Goupil<sup>1</sup>, H. Hess<sup>18</sup>, A. Jungclaus<sup>21</sup>, A. Kaşkaş<sup>22</sup>, A. Korichi<sup>15</sup>, S.M. Lenzi<sup>23,24</sup>, S. Leoni<sup>10,25</sup>, H. Li<sup>1</sup>, J. Ljungvall<sup>15</sup>, A. Lopez-Martens<sup>15</sup>, R. Menegazzo<sup>23</sup>, D. Mengoni<sup>23,24</sup>, B. Million<sup>10</sup>, J. Mrázek<sup>26</sup>, D.R. Napoli<sup>27</sup>, A. Navin<sup>1</sup>, J. Nyberg<sup>28</sup>, Zs. Podolyak<sup>29</sup>, A. Pullia<sup>10,25</sup>, B. Quintana<sup>30</sup>, D. Ralet<sup>1,15</sup>, N. Redon<sup>17</sup>, P. Reiter<sup>18</sup>, K. Rezynkina<sup>31</sup>, F. Saillant<sup>1</sup>, M.D. Salsac<sup>32</sup>, A.M. Sánchez-Benítez<sup>33</sup>, E. Sanchis<sup>20</sup>, M. Şenyiğit<sup>22</sup>, M. Siciliano<sup>32,2</sup>, N.A. Smirnova<sup>34</sup>, D. Sohler<sup>19</sup>, M. Stanoiu<sup>35</sup>, Ch. Theisen<sup>32</sup>, J.J. Valiente-Dobón<sup>27</sup>, P. Ujic<sup>12</sup> and M. Zielińska<sup>32</sup>

<sup>1</sup>Grand Accélérateur National d'Ions Lourds (GANIL),  
CEA/DRF-CNRS/IN2P3, Caen, France.

<sup>2</sup>Physics Division, Argonne National Laboratory, Lemont (IL),  
USA.

<sup>3</sup>Departament de Física, EEBE, Universitat Politècnica de  
Catalunya, Barcelona, Spain.

<sup>4</sup>Institut d'Estudis Espacials de Catalunya, Barcelona, Spain.

<sup>5</sup>Institut Laue-Langevin, Grenoble, France.

<sup>6</sup>Center for Exotic Nuclear Studies, Institute for Basic Science,  
Daejeon, Republic of Korea.

<sup>7</sup>Instituto de Física, Universidade de São Paulo, CEP 05508-090,  
São Paulo, Brazil.

- <sup>8</sup>CERN, Geneva, Switzerland.
- <sup>9</sup>Helmholtz-Zentrum Dresden-Rossendorf, Institute of Ion Beam Physics and Materials Research, Dresden, Germany.
- <sup>10</sup>Istituto Nazionale di Fisica Nucleare, Sezione di Milano, Milano, Italy.
- <sup>11</sup>Oliver Lodge Laboratory, University of Liverpool, Liverpool, United Kingdom.
- <sup>12</sup>Vinca Institute of Nuclear Sciences, University of Belgrade, Belgrade, Serbia.
- <sup>13</sup>Department of Physics, KTH Royal Institute of Technology, Stockholm, Sweden.
- <sup>14</sup>Institute of Nuclear Physics, Kraków, Poland.
- <sup>15</sup>Laboratoire de Physique des 2 Infinis Irène Joliot-Curie, CNRS/IN2P3, Université Paris-Saclay, Orsay, France.
- <sup>16</sup>Instituto de Física Corpuscular, CSIC-Universidad de Valencia, Valencia, Spain.
- <sup>17</sup>Institut de Physique des 2 Infinis de Lyon, CNRS/IN2P3, Université Claude Bernard de Lyon 1, Villeurbanne, France.
- <sup>18</sup>Institut für Kernphysik, Universität zu Köln, Köln, Germany.
- <sup>19</sup>Institute for Nuclear Research (ATOMKI), Debrecen, Hungary.
- <sup>20</sup>Departamento de Ingeniería Electrónica, Universitat de Valencia, Valencia, Spain.
- <sup>21</sup>Instituto de Estructura de la Materia, CSIC, Madrid, Spain.
- <sup>22</sup>Department of Physics, Faculty of Science, Ankara University, Ankara, Turkey.
- <sup>23</sup>Istituto Nazionale di Fisica Nucleare, Sezione di Padova, Padova, Italy.
- <sup>24</sup>Dipartimento di Fisica e Astronomia, Università degli Studi di Padova, Padova, Italy.
- <sup>25</sup>Dipartimento di Fisica, Università di Milano, Milano, Italy.
- <sup>26</sup>Nuclear Physics Institute of the Czech Academy of Sciences, Řež, Czech Republic.
- <sup>27</sup>Laboratori Nazionali di Legnaro INFN, Legnaro (PD), Italy.
- <sup>28</sup>Department of Physics and Astronomy, Uppsala University, Uppsala, Sweden.
- <sup>29</sup>Department of Physics, University of Surrey, Guildford, United Kingdom.
- <sup>30</sup>Laboratorio de Radiaciones Ionizantes, Departamento de Física Fundamental, Universidad de Salamanca, Salamanca, Spain.

<sup>31</sup>Institut pluridisciplinaire Hubert Curien, Université de Strasbourg, CNRS, Strasbourg, France.

<sup>32</sup>Irfu, CEA, Université Paris-Saclay, Gif-sur-Yvette, France.

<sup>33</sup>Department of Integrated Sciences, Centro de Estudios Avanzados en Física, Matemáticas y Computación (CEAFMC), University of Huelva, Huelva, Spain.

<sup>34</sup>Université de Bordeaux, CNRS/IN2P3, LP2IB, Gradignan, France.

<sup>35</sup>Horia Hulubei National Institute for R&D in Physics and Nuclear Engineering, IFIN-HH Bucharest, Măgurele, Romania.

\*Corresponding author(s). E-mail(s): [cfougeres@anl.gov](mailto:cfougeres@anl.gov); [oliveira@ganil.fr](mailto:oliveira@ganil.fr);

Classical novae are thermonuclear explosions in stellar binary systems, and important sources of  $^{26}\text{Al}$  and  $^{22}\text{Na}$ <sup>1–3</sup>. While  $\gamma$  rays from the decay of the former radioisotope have been observed throughout the Galaxy,  $^{22}\text{Na}$  remains untraceable. The half-life of  $^{22}\text{Na}$  (2.6 yr<sup>4</sup>) would allow the observation of its 1.275 MeV  $\gamma$ -ray line from a cosmic source. However, the prediction of such an observation requires good knowledge of the nuclear reactions involved in the production and destruction of this nucleus<sup>5</sup>. The  $^{22}\text{Na}(p, \gamma)^{23}\text{Mg}$ <sup>5</sup> reaction remains the only source of large uncertainty about the amount of  $^{22}\text{Na}$  ejected. Its rate is dominated by a single resonance on the short-lived state at 7785.0(7) keV in  $^{23}\text{Mg}$ <sup>6</sup>. In the present work, a combined analysis of particle-particle correlations and velocity-difference profiles is proposed to measure femtosecond nuclear lifetimes. The application of this novel method to the study of the  $^{23}\text{Mg}$  states, combining magnetic and highly-segmented tracking  $\gamma$ -ray spectrometers, places strong limits on the amount of  $^{22}\text{Na}$  produced in novae, explains its non-observation to date in  $\gamma$  rays (flux  $< 2.5 \times 10^{-4}$  ph.cm<sup>-2</sup>s<sup>-1</sup><sup>7</sup>), and constrains its detectability with future space-borne observatories.

Nuclear reactions between charged particles in astrophysical environments proceed by quantum tunneling. The measurement of these reactions in the laboratory is very difficult because of the very small cross sections ( $\sigma \lesssim 1$  nb). To date, about ten reactions involving radioactive nuclei and charged particles have been directly measured at low energies. Among them, the  $^{22}\text{Na}(p, \gamma)^{23}\text{Mg}$  reaction has a direct impact on the amount of radioactive  $^{22}\text{Na}$  produced in novae<sup>6,8–11</sup>. The astrophysical relevance of  $^{22}\text{Na}$  for diagnosis of nova outbursts was first mentioned by Clayton and Hoyle<sup>3</sup>, in the context of its decay into a

short-lived excited state of  $^{22}\text{Ne}$ , and the subsequent emission of a  $\gamma$ -ray photon of 1.275 MeV released during its de-excitation. A precise determination of the  $^{22}\text{Na}(p, \gamma)^{23}\text{Mg}$  thermonuclear rate is necessary to improve the predicted abundances of nuclei in the mass region  $A \geq 20$  during nova outbursts, including the  $^{22}\text{Na}$  abundance in the ejecta that impacts in turn the predicted  $^{20}\text{Ne}/^{22}\text{Ne}$  ratios in presolar grains<sup>12</sup> of a putative nova origin, as well as, the corresponding  $\gamma$ -ray emission flux. The rate of this reaction is mainly dictated by a single resonance in  $^{23}\text{Mg}$  at 7785.0(7) keV<sup>6</sup>. A direct measurement of its strength ( $\omega\gamma$ ) has been performed in three different studies with conflicting results:  $\omega\gamma = 5.7_{-0.9}^{+1.6}$  meV<sup>6</sup>, 1.4(3) meV<sup>13</sup> and  $< 0.36$  meV<sup>14</sup>. Indirect experimental methods, such as lifetime measurement, have also been employed to determine the strength of this resonance. It has been shown that the ejected mass of  $^{22}\text{Na}$  in novae is inversely proportional to the lifetime of the key state<sup>6</sup>. The lifetime of this state ( $\tau$ ) was previously measured to be  $\tau = 10(3)$  fs<sup>11</sup>, consistent with the recently determined upper limit of 12 fs<sup>15</sup>. Yet, this is at odds with the predictions of the nuclear Shell Model (*SM*),  $\tau_{SM} \approx 1$  fs. Here we propose an experimental method for measuring such short lifetimes. This method has been applied to the key state in  $^{23}\text{Mg}$  in order to obtain an independent measurement and, so, to reduce systematic errors.

The experiment was performed at GANIL, France. A  $^{24}\text{Mg}$  beam was accelerated to 110.8(4) MeV and impinged on a  $^3\text{He}$  target of  $\approx 2 \times 10^{17}$  atoms/cm<sup>2</sup> uniformly implanted up to a depth of 0.1  $\mu\text{m}$  below the surface of a 5.0(5)  $\mu\text{m}$  gold foil, producing the  $^{23}\text{Mg}$  nucleus by the  $^3\text{He}(^{24}\text{Mg}, ^4\text{He})^{23}\text{Mg}$  reaction. Both  $^{24}\text{Mg}$  and  $^{23}\text{Mg}$  nuclei were then stopped in a 20.0(5)  $\mu\text{m}$  gold foil. About twenty states were populated in  $^{23}\text{Mg}$  with excitation energies between 0 and 8 MeV. The light particles produced by the reaction were identified and measured with the VAMOS++ magnetic spectrometer<sup>16</sup> placed at 0° with respect to the beam direction, using 2 drift chambers, a plastic scintillator and 2 small drift chambers placed at the entrance of the spectrometer. This led to an unambiguous identification of the  $^4\text{He}$  particles. The  $^4\text{He}$  particles were detected up to an angle in the laboratory of 10.0(5)° relative to the beam axis. Excitation energy ( $E_x$ ), velocity at the time of the reaction ( $\beta_{\text{reac}} = v_{\text{reac}}/c$ ), and angle of the  $^{23}\text{Mg}$  nuclei ( $\theta_{\text{recoil}}$ ), have been determined by measuring the momentum of the  $^4\text{He}$  ejectiles, with a resolution (FWHM) of  $\approx 500$  keV,  $\approx 0.0005$  and  $\approx 0.05^\circ$  respectively.

The excited states in  $^{23}\text{Mg}$  have been also clearly identified via their  $\gamma$ -ray transitions measured with the AGATA  $\gamma$ -ray spectrometer. The present experimental method has taken advantage of the highest angle sensitivity of AGATA<sup>17,18</sup>. This  $\gamma$ -ray spectrometer is based on  $\gamma$ -ray tracking techniques in highly-segmented HPGe detectors. It consisted of 31 crystals covering an angular range from 120° to 170°, with a total geometrical efficiency  $\approx 0.6 \pi$ . With AGATA, it is possible to measure accurately the energy and the emission angle of the  $\gamma$  rays with a resolution of 4.4(1) keV at 7 MeV and 0.7(1)°, respectively. The  $\gamma$  rays were observed Doppler shifted since they were emitted from a  $^{23}\text{Mg}$  nucleus moving at a certain velocity  $\beta_{\text{ems}} = v_{\text{ems}}/c$ . The measured energy  $E_\gamma$

is a function of the rest energy  $E_{\gamma,0}$  and of the angle  $\theta$  between the  $\gamma$  ray and the  $^{23}\text{Mg}$  emitting nucleus:  $E_{\gamma} = E_{\gamma,0}\sqrt{1 - \beta_{ems}^2}/(1 - \beta_{ems}\cos(\theta))$ . With AGATA, this relativistic Doppler effect can be observed continuously as a function of the angle, as shown in Fig. 1 for the case of the  $E_{\gamma,0} = 4840.0_{-0.4}^{+0.2}$  keV  $\gamma$ -ray transition emitted from the  $E_x = 5292.0(6)$  keV excited state in  $^{23}\text{Mg}$  moving with  $\beta_{ems} \approx 0.075$ . Conversely, if the rest energy of the  $\gamma$  ray is known,

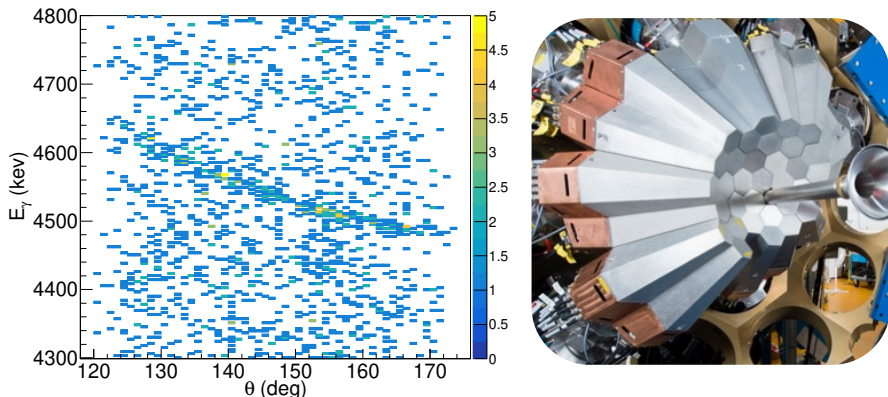


**Fig. 1 Identification of  $\gamma$ -ray transitions in  $^{23}\text{Mg}$ .** Left: The energy of the measured  $\gamma$  rays is plotted as a function of the angle between the  $\gamma$  ray and the  $^{23}\text{Mg}$  emitter. This matrix is conditioned with the detection of an  $\alpha$  particle at  $5.2 < E_x < 5.4$  MeV in the VAMOS++ magnetic spectrometer. The  $\gamma$ -ray transition ( $E_{\gamma,0} = 4840.0_{-0.4}^{+0.2}$  keV) from the  $E_x = 5292.0(6)$  keV excited state in  $^{23}\text{Mg}$  is clearly observed. Its energy is Doppler shifted. The background observed here is mostly due to random coincidences between  $\gamma$  rays from the Compton background and  $\alpha$  particles produced in fusion-evaporation reactions between the beam and  $^{12}\text{C}$  and  $^{16}\text{O}$  impurities deposited on the target. Right: Picture of the AGATA  $\gamma$ -ray spectrometer used to detect the  $\gamma$  rays emitted during the reaction.

it is possible to determine the nucleus velocity at the time of emission  $\beta_{ems}$  from the measured  $E_{\gamma}$  and  $\theta$  (see Methods, section *Determination of velocities*). Their precise measurement, enabled by the combination of both AGATA and VAMOS++, has allowed for the accurate determination of  $\beta_{ems}$ , on a event-by-event basis.

In the present work, both velocities  $\beta_{ems}$  and  $\beta_{reac}$  were measured simultaneously, on a event-by-event basis. The two velocities are not identical since (i) the  $^{23}\text{Mg}$  nucleus slows down in the target before being stopped ( $\approx 500$  fs) and (ii) there is a time difference between the reaction and the  $\gamma$ -ray emission due to the finite lifetime of the state. Thus, the profile of the velocity differences,  $\Delta\beta = \beta_{reac} - \beta_{ems}$ , is a function of the lifetime of the state - a longer lifetime gives a larger value of  $\Delta\beta$ . The technique proposed here, for measuring femtosecond lifetimes, is based on the analysis of velocity-difference profiles.

The results obtained in this work are shown in Fig. 2 for three different excited states of  $^{23}\text{Mg}$ . On the left side,  $\beta_{reac}$  is shown as a function of  $\beta_{ems}$ , and on the right side, the yields of the corresponding  $\gamma$  rays as a function of

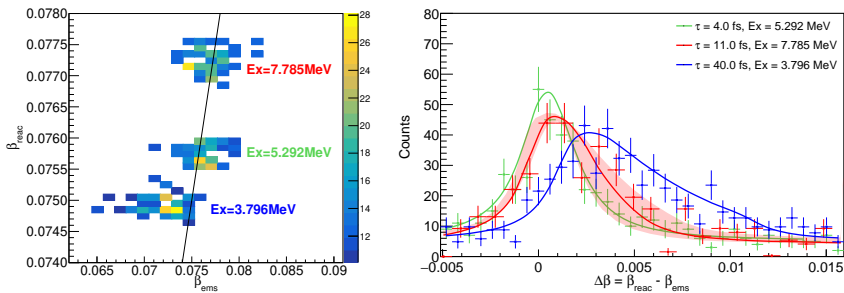


**Fig. 2 Angle-integrated velocity-difference profiles.** Left: the  $^{23}\text{Mg}$  velocity at the time of reaction ( $\beta_{reac}$ ) is shown against the velocity at the time of the  $\gamma$ -ray emission ( $\beta_{ems}$ ), for three excited states. The line corresponds to the prompt  $\gamma$ -ray emission when  $\beta_{ems} = \beta_{reac}$ . The points observed on the left of the line ( $\beta_{ems} < \beta_{reac}$ ) correspond to delayed  $\gamma$ -ray emissions. Right: the corresponding angle-integrated velocity-difference profiles for the three states compared with simulations (continuous lines). It shows unambiguously that the astrophysical state (in red) has a lifetime  $4 < \tau < 40$  fs. The red shaded area corresponds to  $1\sigma$  uncertainty on the lifetime, the horizontal error bars correspond to the width of the bins, which are larger than the real experimental uncertainty, and the vertical error bars to the statistical uncertainty.

the velocity difference  $\Delta\beta$ . The overall shape of the  $\Delta\beta$  measured profiles can be explained in a simple way. The  $\gamma$  rays are emitted following the exponential decay law, i.e.  $N(t) = N_0 \times e^{-\Delta t/\tau}$ , with  $\tau$  being the lifetime of the state and  $\Delta t$  the time elapsed after the reaction. For short lifetimes ( $\tau \lesssim 100$  fs), in the non-relativistic approximation, the deceleration force acting on the  $^{23}\text{Mg}$  ions is almost constant, and consequently  $\Delta\beta \propto \Delta t$ . Therefore, the right side tail of the curves in Fig. 2 (right) would follow the exponential decay function  $N(t) \propto e^{-\Delta\beta/\tau}$ . This explains the asymmetric shape of the profile shown in blue, which corresponds to  $\tau = 40$  fs. Moreover, the experiment has a resolution in  $\Delta\beta$ , i.e.  $0.0032(1)$ , which is measured by the width of the almost Gaussian profile observed for very short lifetimes, see the green profile for  $\tau = 4$  fs in Fig. 2 (right). The overall shape of the measured  $\Delta\beta$  distributions is the convolution of the exponential decay with a Gaussian function. The sensitivity of the method, governed by the statistics, can be better than the resolution of  $\Delta\beta$ . This makes the method sensitive to very short lifetimes, down to 0.8 fs according to simulations. From comparison of the data with Monte Carlo simulations, shown in Fig. 2 (right) by the continuous lines (see also the Supplementary section), the best agreement is obtained with lifetimes of  $4_{-3}^{+1}$  fs and  $40_{-7}^{+6}$  fs for the states  $E_x = 5292.0(6)$  keV ( $E_{\gamma,0} = 4840.1_{-0.4}^{+0.2}$  keV) and  $E_x = 3796.0(1.2)$  keV ( $E_{\gamma,0} = 3344.8_{-1.0}^{+0.8}$  keV), respectively, which is in excellent agreement with their known values of 5(2) fs<sup>4</sup> and 41(6) fs<sup>4</sup>. This shows that the present method is a powerful tool to determine lifetimes in the femtosecond range. With the same method, it is also possible to accurately measure the rest energy of the  $\gamma$ -ray transitions. For the transition from the key state, we measured  $E_{\gamma,0} = 7333.0_{-0.2}^{+0.5}$  keV, in good agreement with the referenced value of  $E_{\gamma,0} = 7333.2(11)$  keV<sup>4</sup>.

The present method has many advantages. Since the excitation energy of the state is precisely selected with VAMOS++, we can ignore any possible top-feeding contribution to the state, and, therefore, the measure is not affected by the lifetime of higher-lying states. Moreover, this method is independent of the reaction mechanism populating the states, i.e. direct transfer or compound-nucleus formation ( $^{24}\text{Mg}+^3\text{He} \rightarrow ^{27}\text{Si}^* \rightarrow ^{23}\text{Mg}+^4\text{He}$ ). Furthermore, the result does not depend on the angular distribution of the emitted  $\gamma$  ray and of the charged particles, nor on the angle-dependent detection efficiency. A single spectrum concentrates all the statistics of the experiment, which maximizes the signal-to-noise ratio. The main sources of uncertainties and their associated contributions for the 7785.0(7) keV state are presented in Table 1.

**Table 1** Systematic errors (in %) on the lifetime of the  $E_x = 7785.0(7)$  keV state.

Source of error	Error on $\tau$ in %
$\gamma$ -ray energy resolution <sup>1</sup>	15
$\gamma$ -ray absolute angle (1 deg) <sup>2</sup>	12
$\gamma$ -ray angle resolution <sup>1</sup>	12
Stopping powers <sup>3</sup>	10
Beam energy dispersion <sup>1</sup>	6.5
Implementation profile of $^3\text{He}$ ions <sup>3</sup>	6.0
$\gamma$ -ray energy shift during runs <sup>4</sup>	3.5
Transverse spatial dispersion of the beam <sup>1</sup>	0.3
Total	26

<sup>1</sup>Measured during the experiment.

<sup>2</sup>Including the uncertainty in the position of the target.

<sup>3</sup>From SRIM<sup>19</sup>-EVASIONS simulations, considering 20 % uncertainty in stopping powers tables.

<sup>4</sup>From the energy calibration stability measured throughout the experiment.

The result obtained for the lifetime of the astrophysical state is  $\tau = 11_{-5}^{+7}$  fs, including statistical and systematic uncertainties, see Fig. 2, confirming the measured value of Jenkins et al<sup>11</sup> ( $\tau = 10(3)$  fs). The reduced magnetic dipole transition probability  $B(M1)$  was deduced from the measured lifetime assuming a negligible  $E2$  electric quadrupole contribution:  $B(M1) = 0.017_{-0.008}^{+0.011} \mu_N^2$ . This value is among the lowest values measured for  $M1$  transitions. To get an insight from theory, we have performed shell-model calculations in the  $sd$  shell with the well-established phenomenological USDA and USDB<sup>20,21</sup> interactions using the NushellX@MSU code<sup>22</sup>. These calculations confirm that the key state is characterized by a low  $B(M1)$  value of  $0.14 \mu_N^2$ , assuming  $7/2^+$  spin and parity assignment (see the discussion below) and optimum values of the effective proton and neutron g-factors. Although this value is almost a factor of 10 larger than the experimentally determined one, the difference is not far from the typical rms error on  $M1$  transition probabilities established for the  $sd$  shell with these interactions<sup>23,24</sup>. Therefore, it can be said that



the measured values of the lifetime are compatible with each other and with shell-model calculations.

The measured lifetime was used to determine the strength of the resonance:  $\omega\gamma = \frac{2J_{23\text{Mg}}+1}{(2J_{22\text{Na}}+1)(2J_p+1)} \times \frac{\Gamma_\gamma\Gamma_p}{\Gamma_\gamma+\Gamma_p} = \omega BR_p(1 - BR_p)\frac{\hbar}{\tau}$ , with  $J$  and  $\Gamma$  being the spin and the partial widths of the key state. Actually, the spin of this state has also been a subject of debate<sup>11,25</sup>, where two values have been proposed:  $J_{23\text{Mg}}^\pi = 7/2^+$ <sup>11</sup> or  $5/2^+$ <sup>25</sup>. We assume it to be  $7/2^+$ . This state is only 18(1.5) keV away from the known  $5/2^+$  isobaric analog state of the <sup>23</sup>Al ground state. In the case of  $5/2^+$  assignment, the states would interfere, as predicted by the nuclear shell-model calculations<sup>24</sup>, and such a mixing has not been observed<sup>6,13,26,27</sup>. Moreover, concerning the  $\gamma$ -ray decay pattern, shell-model calculations agree with a  $7/2^+$  spin<sup>24</sup>. The proton branching ratio,  $BR_p$ , was also measured in this work by detecting protons emitted from the <sup>23</sup>Mg unbound states with an annular silicon detector placed downstream of the target. The obtained value,  $BR_p = 0.68(6)\%$ , is in excellent agreement with the latest published value,  $BR_p = 0.65(8)\%$ <sup>27</sup>.

Combining all measured values into the new recommended values:  $BR_p = 0.67(5)\%$  and  $\tau = 10.2(26)$  fs, results in a consolidated resonance strength of  $\omega\gamma = 0.24_{-0.04}^{+0.11}$  meV, which is compatible with the direct measurement<sup>14</sup> ( $\omega\gamma < 0.36$  meV) but not with the other two direct measurements. It should be pointed out that these direct measurements using radioactive targets are not in agreement with each other, and also that the obtained value is very low, close to the sensitivity limit of these direct experiments. The new value of the resonance strength and a Monte-Carlo approach<sup>28</sup> were used to deduce a new rate for the <sup>22</sup>Na( $p, \gamma$ )<sup>23</sup>Mg reaction (see Fig. 3 and Table 1 in Supplementary). The reliably estimated experimental uncertainties of the present method allowed a more accurate determination of this rate. This new rate was found to be very reliable at maximum nova temperatures, with uncertainties reduced to 40 % (10 %) at T=0.1 GK (0.5 GK). It is worth to mention that if we consider the two possible assignments  $J_{23\text{Mg}}^\pi = (5/2^+, 7/2^+)$ , only a limited increase in the uncertainties is obtained, at most 11% below 0.25 GK.

To quantitatively assess the impact of the new <sup>22</sup>Na( $p, \gamma$ )<sup>23</sup>Mg reaction rate obtained from this work on nova nucleosynthesis, a series of hydrodynamic simulations have been performed. Four physical magnitudes determine the strength of a nova outburst, and, in turn, the synthesis of <sup>22</sup>Na: the white dwarf mass  $M_{\text{WD}}$  (or radius  $R_{\text{WD}}$ ), its initial luminosity  $L_{\text{WD,ini}}$ , the mass-accretion rate  $\dot{M}$ , and the metallicity of the accreted material. The influence of the white dwarf mass on the synthesis of <sup>22</sup>Na has been analyzed. Three different values for the white dwarf mass have been considered: 1.15  $M_\odot$ , 1.25  $M_\odot$ , and 1.35  $M_\odot$ . In these simulations, the star hosting the nova outbursts is assumed to be an ONe white dwarf, with initial luminosity,  $L_{\text{WD,ini}} = 10^{-2} L_\odot$ , and accreting solar composition material<sup>29</sup> from the secondary star at a constant mass-accretion rate of  $\dot{M} = 2 \times 10^{-10} M_\odot/\text{yr}$ . The accreted matter is assumed to mix with material from the outermost white dwarf layers<sup>30</sup>. For consistency

and completeness, the nova outbursts on  $1.15 M_{\odot}$  white dwarfs have been computed with two different, one-dimensional stellar evolution codes: MESA<sup>31–36</sup> and SHIVA<sup>1,37</sup>.

At the early stages of the outburst, when the temperature at the base of the envelope reaches  $T_{\text{base}} \sim 5 \times 10^7$  K, the chain of reactions  $^{20}\text{Ne}(p, \gamma)^{21}\text{Na}(\beta^+)^{21}\text{Ne}(p, \gamma)^{22}\text{Na}$  powers a rapid rise in the  $^{22}\text{Na}$  abundance. When the temperature reaches  $T_{\text{base}} \sim 8 \times 10^7$  K,  $^{22}\text{Na}(p, \gamma)^{23}\text{Mg}$  becomes the main destruction channel. At  $T_{\text{base}} \sim 10^8$  K,  $^{22}\text{Na}(p, \gamma)^{23}\text{Mg}$  becomes the most important reaction involved in the synthesis and destruction of  $^{22}\text{Na}$ , and therefore, its abundance begins to decrease. When  $T_{\text{base}} \sim 2 \times 10^8$  K,  $^{21}\text{Na}(p, \gamma)^{22}\text{Mg}$  becomes faster than  $^{21}\text{Na}(\beta^+)^{21}\text{Ne}$ , such that  $^{20}\text{Ne}(p, \gamma)^{21}\text{Na}(p, \gamma)^{22}\text{Mg}(\beta^+)^{22}\text{Na}$  takes over as the dominant path, favoring the synthesis of  $^{22}\text{Na}$ , which achieves a second maximum after the temperature peak  $T_{\text{peak}}$ . This pattern continues up to  $^{22}\text{Na}(p, \gamma)^{23}\text{Mg}$  becomes again the most relevant reaction when the temperature drops. During the subsequent and final expansion and ejection stages, as the temperature drops dramatically, the evolution of  $^{22}\text{Na}$  is fully governed by  $^{22}\text{Na}(\beta^+)^{22}\text{Ne}$ . The most relevant results obtained in these simulations are summarized in Table 2.

The larger peak temperatures achieved during nova outbursts on more mas-

**Table 2** Abundances of (Ne, Na) isotopes in the ejecta obtained for different nova models calculated with the MESA and SHIVA codes. See text for the parameters.

Model	115a	115b	125	135
HD Code	MESA	SHIVA	SHIVA	SHIVA
$M_{\text{WD}} (M_{\odot})$	1.15	1.15	1.25	1.35
$R_{\text{WD}} (\text{km})$	4428	4334	3797	2258
$T_{\text{peak}} (10^8 \text{ K})$	2.12	2.27	2.48	3.13
$M_{\text{ejec}} (10^{-5} M_{\odot})$	4.63	2.46	1.90	0.46
$X(^{20}\text{Ne})$	$1.4 \times 10^{-1}$	$1.8 \times 10^{-1}$	$1.8 \times 10^{-1}$	$1.5 \times 10^{-1}$
$X(^{21}\text{Ne})$	$2.3 \times 10^{-5}$	$3.6 \times 10^{-5}$	$3.9 \times 10^{-5}$	$4.1 \times 10^{-5}$
$X(^{22}\text{Ne})$	$1.9 \times 10^{-3}$	$1.3 \times 10^{-3}$	$6.4 \times 10^{-4}$	$3.3 \times 10^{-5}$
<b><math>X(^{22}\text{Na})</math></b>	<b><math>3.1 \times 10^{-4}</math></b>	<b><math>3.2 \times 10^{-4}</math></b>	<b><math>3.7 \times 10^{-4}</math></b>	<b><math>9.1 \times 10^{-4}</math></b>
$X(^{23}\text{Na})$	$8.2 \times 10^{-4}$	$9.9 \times 10^{-4}$	$1.1 \times 10^{-3}$	$3.4 \times 10^{-3}$

sive white dwarfs yield larger mean, mass-averaged abundances of  $^{22}\text{Na}$  in the ejecta. However, it is worth noting that the total mass of  $^{22}\text{Na}$  ejected in a nova outburst decreases with the white dwarf mass ( $8 \times 10^{-9} M_{\odot}$ , for Model 115b,  $7 \times 10^{-9} M_{\odot}$ , for Model 125, and  $4.2 \times 10^{-9} M_{\odot}$ , for Model 135), since more massive white dwarfs accrete and eject smaller amounts of mass, see  $M_{\text{ejec}}$  in Table 2.

The new and reliable reaction rate obtained in this work also opens the door to further advanced sensitivity studies on astrophysical parameters, performed here for the first time. The flux has been obtained in a series of nova simulations for a large range of mass-accretion rates  $\dot{M}$  and white dwarf luminosities  $L_{\text{WD,ini}}$ . For example, Fig. 3 shows the expected flux of  $^{22}\text{Na}$  for a nova

event located 1 kpc from the Earth, with  $M_{\text{WD}}=1.2 M_{\odot}$  and accreting solar composition material. This figure shows that the amount of  $^{22}\text{Na}$  does depend on the two parameters, varying smoothly by up to a factor of 3. The change is abrupt only on the lower right side of the figure. In this region, the  $^{22}\text{Na}/^{22}\text{Mg}$  and  $^{22}\text{Na}/^{21}\text{Ne}$  ratios around the peak temperatures have the same values as in the other regions, which means that the production pathways are unchanged. On the contrary, the  $^{23}\text{Mg}/^{22}\text{Na}$  ratio is found 4 times larger, indicating that the destruction by the  $^{22}\text{Na}(p, \gamma)^{23}\text{Mg}$  reaction is more intense in this region. This graph provides a link between the unknown astrophysical parameters of the novae and the measured  $^{22}\text{Na}$  flux. In the future, precise measurements of the  $^{22}\text{Na}$   $\gamma$ -ray flux will constrain these astrophysical parameters.

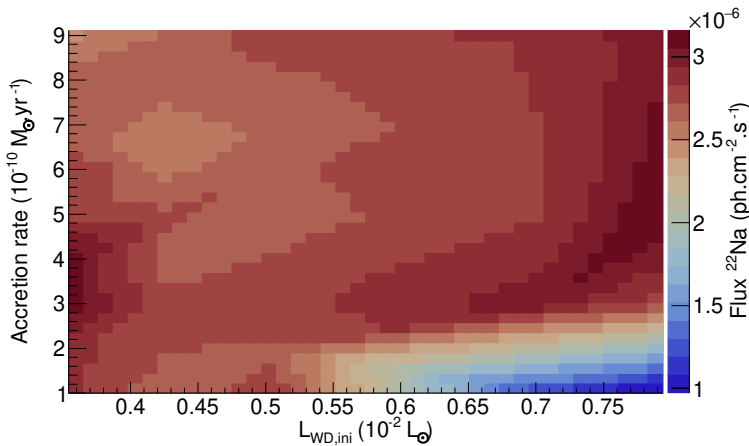


**Fig. 3 Prediction of the 1.275 MeV  $\gamma$ -ray flux emitted from a nova.** The  $^{22}\text{Na}$   $\gamma$ -ray emission flux is shown as a function of the white dwarf initial luminosity and the mass-accretion rate. This is calculated from the  $^{22}\text{Na}$  mass-averaged abundance within the ejected shells. Computations were done for a  $1.2 M_{\odot}$  One white dwarf located 1 kpc from the Earth, using the MESA code<sup>31–36</sup>.

New instruments for  $\gamma$ -ray astronomy are under study or under construction: ESA’s enhanced e-ASTROGAM<sup>38</sup> and NASA’s Compton Spectrometer and Imager, COSI<sup>39</sup>. Both are, in principle, capable of detecting the 1.275 MeV  $\gamma$  rays released in the decay of  $^{22}\text{Na}$  produced in nova outbursts, since they are being designed with a higher efficiency than the past missions, INTEGRAL-SPI<sup>40</sup> and COMPTEL-CGRO<sup>41</sup>. The very high precision in the determination of the  $^{22}\text{Na}(p, \gamma)^{23}\text{Mg}$  rate reported in this work allows to derive, for the first time, realistic estimates of the maximum detectability distance of novae in  $\gamma$  rays, through the 1.275 MeV line. With the expected sensitivities of e-ASTROGRAM ( $3 \times 10^{-6}$  photons  $\text{cm}^{-2} \text{s}^{-1}$ ) and COSI ( $1.7 \times 10^{-6}$  photons  $\text{cm}^{-2} \text{s}^{-1}$ ) at 1 MeV, and assuming that  $\sim 7 \times 10^{-9} M_{\odot}$  of  $^{22}\text{Na}$  are ejected in a typical nova outburst (model 125, Table 2), new maximum detectability distances of 2.7 kpc and 4.0 kpc, respectively, have been derived. These

new estimates suggest a large chance for the possible detection of the  $^{22}\text{Na}$   $\gamma$  rays produced in an ONe nova by the next generation of space-borne  $\gamma$ -ray observatories.

In addition to the results obtained for the astrophysical state, new experimental results were obtained for about twenty  $^{23}\text{Mg}$  states observed in this study and will be the subject of a future publication. The present method is more universal than the conventional Doppler Shift Attenuation Method (DSAM)<sup>42–44</sup>. Unlike DSAM where  $\beta_{reac}$  is not experimentally accessed and its change in the target a source of uncertainty, in the present method a thick target can be used since  $\beta_{reac}$  and  $\beta_{ems}$  are determined for each event. This feature explains the low sensitivity of the obtained results to the  $^3\text{He}$  initial implementation profile and its evolution with time, as shown in Table 1. Indeed, measuring  $\beta_{reac}$  during the experiment, event by event, is equivalent to measuring the reaction point, and therefore, to an on-line measurement of the  $^3\text{He}$  profile in the target and its evolution. Moreover, if the state decays mainly by proton emission instead of  $\gamma$  ray, it is possible to determine its lifetime with the same method using  $\alpha - p$  correlations. The protons are kinetically boosted at forward angles as the  $\gamma$  rays are Doppler shifted. From this kinetic-boost effect, it is possible to determine the velocity  $\beta_{ems}$  of the nucleus at the proton-emission time and to deduce the lifetime of the state with femtosecond accuracy. In addition, it is possible to constrain the spin of the state using the particle-particle correlation analysis method<sup>45</sup>, by measuring the angular distribution of the second emitted particle, proton or  $\gamma$ , over a wide range of angles. It might be interesting to also measure the  $^{23}\text{Mg}$  recoil nuclei. On the one hand the magnetic rigidity of  $^{23}\text{Mg}$  is very different from that of the primary beam, so it could be easy to measure these nuclei with a magnetic spectrometer. On the other hand, the background noise generated by fusion-evaporation reactions could be much less with the measurement and identification of the recoil nuclei. All these advantages, obtained or achievable with remarkable detectors like AGATA and VAMOS++, make this method a promising way to measure in the future other excited states with femtosecond lifetimes.

## Methods

**Determination of velocities.** The velocity  $\beta_{reac}$  of the  $^{23}\text{Mg}$  nuclei at the reaction time was derived from the momentum of the  $\alpha$  particles measured with the VAMOS++ magnetic spectrometer and from the kinematics laws of energy and momentum conservation in the case of the  $^3\text{He}(^{24}\text{Mg},\alpha)^{23}\text{Mg}$  two-body reaction

$$\beta_{reac} = \sqrt{1 - \gamma_{reac}^{-2}}$$

with

$$\gamma_{reac} = \sqrt{1 + \frac{\frac{m_{\alpha}^2 \beta_{\alpha}^2}{1 - \beta_{\alpha}^2} + \frac{m_{beam}^2 \beta_{beam}^2}{1 - \beta_{beam}^2} - 2 \cos(\theta_{\alpha}) m_{beam} m_{\alpha} \sqrt{\gamma_{\alpha}^2 - 1} \sqrt{\gamma_{beam}^2 - 1}}{m_{recoil}^2}} \quad (1)$$

where  $m_{\alpha}$ ,  $m_{beam}$  and  $m_{recoil}$  are the rest-mass energies of the  $\alpha$ ,  $^{24}\text{Mg}$  and  $^{23}\text{Mg}$  nuclei,  $\theta_{\alpha}$  the angle between the  $\alpha$  particle and the beam axis. The parameter  $\gamma_{\alpha}$  was measured with VAMOS++ and corrected for the energy losses in the target using the SRIM code<sup>19</sup>. The parameter  $\gamma_{beam}$ , measured prior to the experiment, was then determined from the measured  $\gamma_{\alpha}$  and a  $\gamma$ -ray transition detected in coincidence.

The velocity  $\beta_{ems}$  of the  $^{23}\text{Mg}$  nuclei at the  $\gamma$ -ray emission time was derived from the measured  $\gamma$  rays. Since the  $^{23}\text{Mg}$  nuclei are moving at the time of the  $\gamma$ -ray emission, the  $\gamma$ -ray energy is Doppler shifted, with the measured energies  $E_{\gamma}$  shifted from the rest energy  $E_{\gamma,0}$  according to

$$E_{\gamma} = E_{\gamma,0} \frac{\sqrt{1 - \beta_{ems}^2}}{1 - \beta_{ems} \cos(\theta)} \quad (2)$$

It follows that

$$\beta_{ems} = \frac{R^2 \cos(\theta) + \sqrt{1 + R^2 \cos^2(\theta) - R^2}}{R^2 \cos^2(\theta) + 1} \quad (3)$$

with  $R = E_{\gamma}/E_{\gamma,0}$ . Here,  $R < 1$  since the AGATA detector was located upstream of the target. The angle  $\theta$  between the  $\gamma$  ray and the  $^{23}\text{Mg}$  recoil nucleus was derived from the measured  $(\theta, \phi)$  of the  $\gamma$  ray and the  $\alpha$  particle using the formulas

$$\begin{aligned} \cos(\theta) = & \sin(\theta_{\gamma}) \sin(\theta_{recoil}) [\cos(\phi_{\gamma}) \cos(\phi_{recoil}) + \sin(\phi_{\gamma}) \sin(\phi_{recoil})] \\ & + \cos(\theta_{\gamma}) \cos(\theta_{recoil}) \end{aligned}$$

where

$$\begin{aligned} \theta_{recoil} = & \text{acos}\left(\frac{m_{beam} \sqrt{\gamma_{beam}^2 - 1} - m_{\alpha} \cos(\theta_{\alpha}) \sqrt{\gamma_{\alpha}^2 - 1}}{m_{recoil} \sqrt{\gamma_{recoil}^2 - 1}}\right) \\ \phi_{recoil} = & \pi + \phi_{\alpha} \end{aligned} \quad (4)$$

**Fit of velocity-difference profiles.** Velocity-difference profiles were numerically simulated with a Monte-Carlo approach developed in the EVASIONS C++/ROOT code. The principle of these numerical simulations will be the subject of a future publication. Simulated velocity-difference profiles were normalized to the measured ones via the profile integrals. The goodness of fit between experimental and simulated profiles was quantified with the

Pearson  $\chi^2$  tests where the lifetime and the  $\gamma$ -ray rest energy are taken as free parameters.

**Branching ratios.** The  $E_x = 7785.0(7)$  keV astrophysical state can decay via proton or  $\gamma$ -ray emission. Therefore, after applying a selection on  $E_x$  in  $^{23}\text{Mg}$  by using the measured  $\alpha$  particles, the number of detected protons and  $\gamma$  rays allowed us to determine the proton and  $\gamma$ -ray branching ratios. These values were corrected for the detection efficiencies. On the one hand, the geometrical efficiency of the silicon detector was estimated by numerical simulations. The angular distribution was considered isotropic for the emitted  $\ell=0$  protons. On the other hand, the AGATA efficiency was measured at low energies with a radioactive  $^{152}\text{Eu}$  source, and simulated with the AGATA `Geant4` code library<sup>46,47</sup> to determine the efficiency at high energies after scaling the simulations to the measured efficiencies at low energies.

**Determination of the  $^{22}\text{Na}$  flux in novae.** The amount of  $^{22}\text{Na}$  ejected in a nova outburst was obtained with the simulation codes MESA<sup>31–35</sup> and SHIVA<sup>1,37</sup> from its abundance in the ejected layers. MESA and SHIVA use several criteria for the ejection of a specific layer, based either on achieving escape (velocity) or a luminosity above the Eddington limit where the radiative pressure exceeds the gravitational force.

**Data availability.** The experimental data of this work related to particles measurements are available upon reasonable request by contacting the primary author. Due to the large size of the data, they cannot be hosted publicly. The ownership of data generated by the AGATA  $\gamma$ -ray spectrometer resides with the AGATA collaboration as detailed in the AGATA Data Policy<sup>48</sup>.

**Codes availability.** The EVASIONS code used in this study is available from the primary author upon reasonable request. Other codes employed here, i.e. SRIM<sup>19</sup>, NushellX@MSU<sup>22</sup>, MESA<sup>31–35</sup> and RatesMC<sup>28</sup>, are freely available.

## References

1. José, J. *Stellar Explosions: Hydrodynamics and Nucleosynthesis*. CRC, Taylor and Francis, Boca Raton, FL, USA **10**, b19165 (2016) .
2. Bode, M. F. & Evans, A. Classical novae. *Classical Novae* **43** (2008) .
3. Clayton, D. D. & Hoyle, F. Gamma-ray lines from novae. *Astrophys. J.* **187**, L101 (1974) .
4. Shamsuzzoha Basunia, M. & Chakraborty, A. Nuclear data sheets for A=23. *Nucl. Data Sheets* **171**, 1–252 (2021). <https://doi.org/10.1016/j.nds.2020.12.001> .

5. José, J., Hernanz, M. & Iliadis, C. Nucleosynthesis in classical novae. *Nucl. Phys. A* **777**, 550–578 (2006). <https://doi.org/10.1016/j.nuclphysa.2005.02.121>, special Issue on Nuclear Astrophysics .
6. Sallaska, A. L. *et al.* Direct Measurements of  $^{22}\text{Na}(p,\gamma)^{23}\text{Mg}$  Resonances and Consequences for  $^{22}\text{Na}$  Production in Classical Novae. *Phy. Rev. Lett.* **105**, 152501 (2010). <https://doi.org/10.1103/PhysRevLett.105.152501> .
7. Diehl, R. Cosmic gamma-ray spectroscopy. *Astronomical Review* **8** (3), 19–65 (2013). <https://doi.org/10.1080/21672857.2013.11519722> .
8. José, J., Coc, A. & Hernanz, M. Nuclear Uncertainties in the NeNa-MgAl Cycles and Production of  $^{22}\text{Na}$  and  $^{26}\text{Al}$  during Nova Outbursts. *Astrophys. J.* **520**, 347–360 (1999). <https://doi.org/10.1086/307445> .
9. Iliadis, C., Champagne, A., José, J., Starrfield, S. & Tupper, P. The Effects of Thermonuclear Reaction-Rate Variations on Nova Nucleosynthesis: A Sensitivity Study. *Astrophys. J. Suppl. Ser.* **142**, 105–137 (2002). <https://doi.org/10.1086/341400> .
10. Hix, W. R., Smith, M. S., Starrfield, S., Mezzacappa, A. & Smith, D. L. Impact of nuclear reaction rate uncertainties on Nova models. *Nucl. Phys. A* **718**, 620–622 (2003). [https://doi.org/10.1016/S0375-9474\(03\)00904-7](https://doi.org/10.1016/S0375-9474(03)00904-7) .
11. Jenkins, D. G. *et al.* Reevaluation of the  $^{22}\text{Na}(p,\gamma)$  Reaction Rate: Implications for the Detection of  $^{22}\text{Na}$  Gamma Rays from Novae. *Phy. Rev. Lett.* **92**, 031101 (2004). <https://doi.org/10.1103/PhysRevLett.92.031101> .
12. Amari, S. *et al.* Presolar grains from novae. *Astrophys. J.* **551** (2), 1065–1072 (2001). <https://doi.org/10.1086/320235> .
13. Stegmüller, F. *et al.*  $^{22}\text{Na}(p,\gamma)^{23}\text{Mg}$  resonant reaction at low energies. *Nucl. Phys. A.* **601**, 168–180 (1996). [https://doi.org/10.1016/0375-9474\(96\)00084-X](https://doi.org/10.1016/0375-9474(96)00084-X) .
14. Seuthe, S. *et al.* Resonances in the  $^{22}\text{Na}(p,\gamma)^{23}\text{Mg}$  reactions. *Nucl. Phys. A.* **514**, 471–502 (1990). [https://doi.org/10.1016/0375-9474\(90\)90153-D](https://doi.org/10.1016/0375-9474(90)90153-D) .
15. Kirsebom, O. S. *et al.* Measurement of lifetimes in  $^{23}\text{Mg}$ . *Phy. Rev. C* **93**, 025802 (2016). <https://doi.org/10.1103/PhysRevC.93.025802> .
16. Rejmund, M. *et al.* Performance of the improved larger acceptance spectrometer: Vamos++. *Nucl. Instrum. Methods Phys. Res. Sect. A: Accel. Spectrom. Detect. Associated Equip.* **646** (1), 184–191 (2011). <https://doi.org/https://doi.org/10.1016/j.nima.2011.05.007> .

17. Akkoyun, S. *et al.* AGATA—Advanced GAMMA Tracking Array. *Nucl. Instrum. Methods Phys. Res. Sect. A: Accel. Spectrom. Detect. Associated Equip.* **668**, 26–58 (2012). <https://doi.org/10.1016/j.nima.2011.11.081> .
18. Clément, E. *et al.* Conceptual design of the AGATA  $1\pi$  array at GANIL. *Nucl. Instrum. Methods Phys. Res. Sect. A: Accel. Spectrom. Detect. Associated Equip.* **855**, 1–12 (2017). <https://doi.org/10.1016/j.nima.2017.02.063> .
19. Ziegler, J. F., Biersack, J. P. & Ziegler, M. D. SRIM - The Stopping and Range of Ions in Matter. (*SRIM Co., United States of America*) **6<sup>th</sup> ed.** (2013) .
20. Brown, B. A. & Richter, W. A. New “USD” Hamiltonians for the  $sd$  shell. *Phys. Rev. C* **74**, 034315 (2006). <https://doi.org/10.1103/PhysRevC.74.034315> .
21. Ormand, W. E. & Brown, B. A. Empirical isospin-nonconserving hamiltonians for shell-model calculations. *Nucl. Phys. A* **491** (1), 1–23 (1989). [https://doi.org/10.1016/0375-9474\(89\)90203-0](https://doi.org/10.1016/0375-9474(89)90203-0) .
22. Brown, B. A. & Rae, W. D. M. The Shell-Model Code NuShellX@MSU. *Nucl. Data Sheets* **120**, 115–118 (2014). <https://doi.org/10.1016/j.nds.2014.07.022> .
23. Richter, W. A., Mkhize, S. & Brown, B. A.  $sd$ -shell observables for the usda and usdb hamiltonians. *Phys. Rev. C* **78**, 064302 (2008). URL <https://link.aps.org/doi/10.1103/PhysRevC.78.064302>. <https://doi.org/10.1103/PhysRevC.78.064302> .
24. Fougères, C. *et al.* Understanding the cosmic abundance of  $^{22}\text{Na}$ : lifetime measurements in  $^{23}\text{Mg}$  (2022). Accepted *EPJ Web of Conferences*, preprint <https://doi.org/10.48550/arXiv.2210.14336>.
25. Kwag, M. S. *et al.* Spin assignments for  $^{23}\text{Mg}$  levels and the astrophysical  $^{22}\text{Na}(p,\gamma)^{23}\text{Mg}$  reaction. *Eur. Phys. J. A* **56**, 108 (2020). <https://doi.org/10.1140/epja/s10050-020-00106-y> .
26. Saastamoinen, A. *et al.* Experimental study of  $\beta$ -delayed proton decay of  $^{23}\text{Al}$  for nucleosynthesis in novae. *Phys. Rev. C* **83**, 045808 (2011). <https://doi.org/10.1103/PhysRevC.83.045808> .
27. Friedman, M. *et al.* Low-energy  $^{23}\text{Al}$   $\beta$ -delayed proton decay and  $^{22}\text{Na}$  destruction in novae. *Phys. Rev. C* **101**, 052802 (2020). <https://doi.org/10.1103/PhysRevC.101.052802> .



28. Longland, R. *et al.* Charged-particle thermonuclear reaction rates: I. Monte Carlo method and statistical distributions. *Nucl. Phys. A* **841**, 1–30 (2010). <https://doi.org/10.1016/j.nuclphysa.2010.04.008> .
29. Lodders, K., Palme, H. & Gail, H. P. Abundances of the Elements in the Solar System. *Springer-Verlag Berlin Heidelberg* **4B**, 712 (2009). [https://doi.org/10.1007/978-3-540-88055-4\\_34](https://doi.org/10.1007/978-3-540-88055-4_34) .
30. Ritossa, C., Garcia-Berro, E. & Iben, J. I. On the Evolution of Stars That Form Electron-degenerate Cores Processed by Carbon Burning. II. Isotope Abundances and Thermal Pulses in a 10  $M_{sun}$  Model with an ONe Core and Applications to Long-Period Variables, Classical Novae, and Accretion-induced Collapse. *Astrophys. J.* **460**, 489 (1996). <https://doi.org/10.1086/176987> .
31. Paxton, B. *et al.* Modules for Experiments in Stellar Astrophysics (MESA). *Astrophys. J. Suppl. Ser.* **192** (1), 3 (2011). <https://doi.org/10.1088/0067-0049/192/1/3> .
32. Paxton, B. *et al.* Modules for Experiments in Stellar Astrophysics (MESA): Planets, Oscillations, Rotation, and Massive Stars. *Astrophys. J. Suppl. Ser.* **208** (1), 4 (2013). <https://doi.org/10.1088/0067-0049/208/1/4> .
33. Paxton, B. *et al.* Modules for Experiments in Stellar Astrophysics (MESA): Binaries, Pulsations, and Explosions. *Astrophys. J. Suppl. Ser.* **220** (1), 15 (2015). <https://doi.org/10.1088/0067-0049/220/1/15> .
34. Paxton, B. *et al.* Modules for Experiments in Stellar Astrophysics (MESA): Convective Boundaries, Element Diffusion, and Massive Star Explosions. *Astrophys. J. Suppl. Ser.* **234** (2), 34 (2018). <https://doi.org/10.3847/1538-4365/aaa5a8> .
35. Paxton, B. *et al.* Modules for Experiments in Stellar Astrophysics (MESA): Pulsating Variable Stars, Rotation, Convective Boundaries, and Energy Conservation. *Astrophys. J. Suppl. Ser.* **243** (1), 10 (2019). <https://doi.org/10.3847/1538-4365/ab2241> .
36. Denissenkov, P. *et al.* MESA and NuGrid simulations of classical novae: CO and ONe nova nucleosynthesis. *Mon. Not. R. Astron. Soc.* **442**, 2058–2074 (2014). <https://doi.org/10.1093/mnras/stu1000> .
37. José, J. & Hernanz, M. Nucleosynthesis in classical novae: CO versus ONe white dwarfs. *Astrophys. J.* **494** (2), 680–690 (1998). <https://doi.org/10.1086/305244> .

38. De Angelis, A. *et al.* Science with e-ASTROGAM. A space mission for MeV-GeV gamma-ray astrophysics. *J. High Energy Astrophys.* **19**, 1–106 (2018). <https://doi.org/10.1016/j.jheap.2018.07.001> .
39. Tomsick, J. *et al.* The Compton Spectrometer and Imager. *Bulletin of the AAS*, 51(7) (2020) .
40. Vedrenne, G. *et al.* Spi: The spectrometer aboard integral. *Astron. Astrophys.* **411** (1) (2003). <https://doi.org/10.1051/0004-6361:20031482> .
41. Schoenfelder, V. *et al.* Instrument Description and Performance of the Imaging Gamma-Ray Telescope COMPTEL aboard the Compton Gamma-Ray Observatory. *Astrophys. J. Suppl. Ser.* **86**, 657 (1993). <https://doi.org/10.1086/191794> .
42. Stahl, C., Leske, J., Lettmann, M. & Pietralla, N. Apcad—analysis program for the continuous-angle dsam. *Comput. Phys. Commun.* **214**, 174–198 (2017). <https://doi.org/https://doi.org/10.1016/j.cpc.2017.01.009> .
43. Nolan, P. J. & Sharpey-Schafer, J. F. The measurement of the lifetimes of excited nuclear states. *Reports on Progress in Physics* **42** (1) (1979). <https://doi.org/10.1088/0034-4885/42/1/001> .
44. Schwarzschild, A. Z. & Warburton, E. K. The measurement of short nuclear lifetimes. *Annual Review of Nuclear Science* **18** (1), 265–290 (1968). <https://doi.org/10.1146/annurev.ns.18.120168.001405> .
45. Pronko, J. & Lindgren, R. Angular correlations of sequential particle decay for aligned nuclei. *Nucl. Instrum. and Methods* **98** (3), 445–449 (1972). [https://doi.org/10.1016/0029-554X\(72\)90226-1](https://doi.org/10.1016/0029-554X(72)90226-1) .
46. Labiche, M. *et al.* AGATA Geant4 simulations Library <http://npg.dl.ac.uk/svn/agata/> (2022).
47. Farnea, E. *et al.* Conceptual design and monte carlo simulations of the agata array. *Nucl. Instrum. Methods Phys. Res. Sect. A: Accel. Spectrom. Detect. Associated Equip.* **621** (1), 331–343 (2010). <https://doi.org/https://doi.org/10.1016/j.nima.2010.04.043> .
48. The AGATA collaboration (2022). [https://www.agata.org/acc/data\\_policy](https://www.agata.org/acc/data_policy).

**Acknowledgments.** The authors thank the GANIL accelerator staff for their beam delivery and support as well as the AGATA collaboration. This work was supported by the Normandie Region, the European project ChETEC-INFRA (101008324) and SPIRAL2-CZ. Y.H.K. would like to acknowledge the support of the Institute for Basic Science (IBS-R031-D1).

M.S. would like to acknowledge that this work has been partially supported by the OASIS project no. ANR-17-CE31-0026 and by the U.S. Department of Energy, Office of Science, Office of Nuclear Physics, under contract number DE-AC02-06CH11357.

**Authors' contributions.** F.O.S. and C.M. were PIs of the experiment during which F.O.S., C.M., E.C., Y.H.K., A.L., V.G., D.B., F.B., I.C., M.C., C.D., J.D., Z.F., S.L., J.L., A.L.M., J.M., D.R., N.R., A.M.S.B, M.S. and P.U. participated in person. Targets making was performed by R.B., C.F., C.M., E.C., A.L., D.B., G.B., A.J.B., A.B., B.C., C.D.P., J.D., J.E., V.G., J.G., H.H., A.J., A.K., A.K., S.M.L., S.L., H.L., J.L., A.L.M., R.M., D.M., B.M., D.R.N., J.N., Zs.P., A.P., B.Q., D.R., P.R., K.R., F.S., M.D.S., E.S., M.S., M.S., D.S., Ch.T., J.J.V.D. and M.Z. have been involved to the AGATA collaboration. Experimental analysis and simulations were undertook by C.F. and F.O.S.. Experimental results were in particular discussed by C.F., F.O.S., E.C., A.L. and A.N.. Theoretical calculations on nuclear structure were done by C.F., N.S. and F.O.S.. Astrophysical calculations and analysis were performed by C.F., J.J. and F.O.S.. F.O.S., C.F. and J.J. were involved in the primary manuscript. All co-authors discussed the final results and contributed to the final manuscript.

**Ethics declarations: competing interests.** The authors declare no competing interests.

**Supplementary information.** Additional information is available in the supplementary section of the paper, in particular fit results, numerical simulations and reaction rate used in the present study.